Korean Journal of Remote Sensing, Vol.21, No.3, 2005, pp.189~211

Application of Multispectral Remotely Sensed Imagery for the Characterization of Complex Coastal Wetland Ecosystems of southern India: A Special Emphasis on Comparing Soft and Hard Classification Methods

Palanisamy Shanmugam†, Yu-Hwan Ahn, and Shanmugam Sanjeevi*

Korea Ocean Research and Development Institute, Seoul 425 600, Korea
Anna University, Chennai 600 025, India*

Abstract : This paper makes an effort to compare the recently evolved soft classification method based on Linear Spectral Mixture Modeling (LSMM) with the traditional hard classification methods based on Iterative Self-Organizing Data Analysis (ISODATA) and Maximum Likelihood Classification (MLC) algorithms in order to achieve appropriate results for mapping, monitoring and preserving valuable coastal wetland ecosystems of southern India using Indian Remote Sensing Satellite (IRS) 1C/1D LISS-III and Landsat-5 Thematic Mapper image data. ISODATA and MLC methods were attempted on these satellite image data to produce maps of 5, 10, 15 and 20 wetland classes for each of three contrast coastal wetland sites, Pitchavaram, Vedaranniyam and Rameswaram. The accuracy of the derived classes was assessed with the simplest descriptive statistic technique called overall accuracy and a discrete multivariate technique called KAPPA accuracy. ISODATA classification resulted in maps with poor accuracy compared to MLC classification that produced maps with improved accuracy. However, there was a systematic decrease in overall accuracy and KAPPA accuracy, when more number of classes was derived from IRS-1C/1D and Landsat-5 TM imagery by ISODATA and MLC. There were two principal factors for the decreased classification accuracy, namely spectral overlapping/confusion and inadequate spatial resolution of the sensors. Compared to the former, the limited instantaneous field of view (IFOV) of these sensors caused occurrence of number of mixture pixels (mixels) in the image and its effect on the classification process was a major problem to deriving accurate wetland cover types, in spite of the increasing spatial resolution of new generation Earth Observation Sensors (EOS). In order to improve the classification accuracy, a soft classification method based on Linear Spectral Mixture Modeling (LSMM) was described to calculate the spectral mixture and classify IRS-1C/1D LISS-III and Landsat-5 TM Imagery. This method considered number of reflectance end-members that form the scene spectra, followed by the determination of their nature and finally the decomposition of the spectra into their end-members. To evaluate the LSMM areal estimates, resulted fractional end-members were compared with normalized difference vegetation index (NDVI), ground truth data, as well as those estimates derived from the traditional hard classifier (MLC). The findings revealed that NDVI values and vegetation fractions were

Received 10 December 2004; Accepted 16 June 2005.
† Corresponding Author: P. Shanmugam (pshanmugam@kordi.re.kr)

positively correlated (r^2 = 0.96, 0.95 and 0.92 for Rameswaram, Vedaranniyam and Pitchavaram respectively) and NDVI and soil fraction values were negatively correlated (r^2 =0.53, 0.39 and 0.13), indicating the reliability of the sub-pixel classification. Comparing with ground truth data, the precision of LSMM for deriving moisture fraction was 92% and 96% for soil fraction. The LSMM in general would seem well suited to locating small wetland habitats which occurred as sub-pixel inclusions, and to representing continuous gradations between different habitat types.

Key Words : IRS-1C/1D LISS-III, Landsat-5 TM, LSMM, Hard and soft classification, Wetlands, Southern India

1. Introduction

The southern Indian coastal zone, an extremely important socio-economic aspect of the country, is endowed with the presence of extensive and diverse mangrove wetlands, marsh, mudflats, sand dunes, lagoons, beaches and coral reefs. Among these, the mangrove wetlands act as a barrier against cyclones, prevent coastal erosion, and provide nursery grounds for a number of commercially-important fish, prawns and crabs, and also play an important role in enhancing the fishery production of the adjacent neritic waters by exporting organic and inorganic nutrients (Shanmugam, 2002; Selvam, 2003). The environmental setting of these multiple-use ecosystems is governed by physical forces such as geomorphology of the coast, climate, tidal amplitude and duration, and quantity of fresh water inflow (Thom, 1984). These wetlands forming habitats for many biological communities are highly dynamic and complex in nature and are fragile ecosystems often being affected both seasonally and annually by various natural and anthropogenic factors, leading to degradation of the habitats. A better understanding of wetland functions under a complex interplay of physical, chemical, biological and geological processes, and mapping and monitoring of ecologically important and sensitive areas of these regions are thus of importance in better coastal zone management (Shanmugam, 2002).

Rapid, repeatable and relatively large-scale environmental monitoring is essential to define spatial patterning and dynamics of wetland vegetation cover and productivity on marsh surfaces, to characterize the changing boundaries between mudflat, marsh, mangrove and sand dune environments, and to provide input into a better understanding of vegetation, soil and topographic interactions on intertidal surfaces. Accomplishing these with the conventional field sampling and surveying is not feasible, because they are time consuming and high cost processes, and moreover some of the areas are not accessible. Thus, establishment of appropriate mapping tools and associated protocols offer the possibility of tracking and monitoring changes in such complex systems of mangrove-marsh-mudflat and sand dunes associated with near-future change in environmental conditions. Spatially extensive and non-invasive remote sensing data due to its synoptic, repetitive and multi-spectral nature provide a wide range of information over inaccessible and larger areas in frequent intervals and has made remote sensing technology a useful tool for mapping and monitoring the wetland conditions, amount of vegetation biomass and the degree of water inundation and conditions (Green *et al.*, 1996; Smith *et al.*, 1998; Ramsey *et al.*, 1999).

Mapping of coastal wetland cover types using remotely sensed data is generally accomplished through image classification techniques such as ISODATA or Maximum Likelihood Classifiers (MLC) (Bolstad and Lillesand, 1991; Franklin, 1994; Ramachandran *et al.*, 1998). These techniques referred to as hard or per-pixel classifiers are, however, not successful in many cases because they assign each pixel to a class through considering its similarities with the class or with other

classes (Jensen, 1996), eventually the mixed pixels are assigned to the most similar class, and mush of the original spectral information can no longer be retrieved from the classified image, thus resulting in decreased classification accuracy. Still visual analysis is often reported to obtain higher accuracy (Martin, 1989; Mas and Ramirez, 1996). As the wetland habitat types appear to be small and continuous with no distinct boundaries, it is therefore desirable to unmix mixed pixel signatures to identify habitat types which are present at the sub-pixel level. Previous studies have demonstrated that soft classification techniques such as Linear Spectral Mixture Modeling (LSMM) and fuzzy classification techniques are likely to give a more accurate map than hard classification techniques (Fisher *et al.*, 1990; Foody *et al.*, 1994; Garcio-Haro *et al.*, 1996; Bastin, 1997; Pu *et al.*, 2003). Of the available soft classifiers, the LSMM is an excellent approximation technique suitable for handing the spectral mixture problem, mainly because (1) it does not require extensive training data, (2) it produces a set of maps, one for each class types concerned, and (3) it was extensively applied to extract the abundance of various components within the mixed pixels of satellite data of similar environments (Robert *et al.*, 1993; Ustin *et al.*, 1996; Cochrane and Souza, 1998; Shanmugam, 2002).

The objective of this paper is to evaluate the accuracy of traditional hard classification methods based on ISODATA and MLC algorithms, and to compare with the recently evolved method based on LSMM for mapping complex coastal wetland cover types of southern India using IRS-1C/1D LISS-III and Landsat-5 TM imagery. The results from applying LSMM were assessed by comparison with those produced by MLC algorithm and with ground truth data, collected from the field survey coincident with the satellite overpass on Pitchavaram and Vedaranniyam wetlands.

2. Study Area, Data and Field Survey

The study area encompassing three different coastal wetland sites in the southern part of India are Pitchavaram, Vedaranniyam and Rameswaram. Pitchavaram coastal wetland lying between the coordinates of latitude 11° 20′ to 11° 30′ N and longitude 79° 45′ to 79° 51′ E (Fig. 1) represents a heterogeneous mixture of mangrove ecosystem. It is an estuarine type of mangrove connected to the Vellar estuary in the north and Coleroon estuary in the south along with the Killai lagoon by a well developed backwater system, which is referred to as the Vellar-Coleroon estuarine complex, and is known for its luxuriant growth of mangrove plants with high productivity and diversity of fauna and is provided with rich detritus, nutrients, salts, vitamins, trace elements etc. The total area of the Vellar-Coleroon estuarine complex is about 2335.5 ha, of which only 241 ha (10.32%) is occupied by dense mangrove vegetation, nearly 593 ha (25.41%) by halophytic vegetations like *Suaeda*, 262.5 ha (11.24%) by barren mud flats, and 1238.5 ha (53.0%) by barren high saline soil. The most dominant mangrove and marsh species are *Rhizophora apiculata, Avicennia marina and Suaeda maritima.* Cattle grazing and felling are mainly responsible for the high degree of degradation of the Pitchavaram mangroves (MSSRF, 1995).

Vedaranniyam wetland is one of the largest coastal wetlands of southern India situated 150km south of Pitchavaram wetland, covering latitude 10° 15′ to 10° 30′ N and longitude 79° 20′ to 79° 53′ E (Fig. 1). It is predominantly formed by marine and partly by fluvial actions, comprising of lagoons, mudflats, marsh with mud/swamp, mangroves, scrubs, sand dunes, spits etc. The tidal swamp forest and mangroves are of evergreen plant communities found along the shores of sheltered creeks, fringes of the lagoons, deltas and islands below the flood tide mark. Six distributaries of the Cauvery

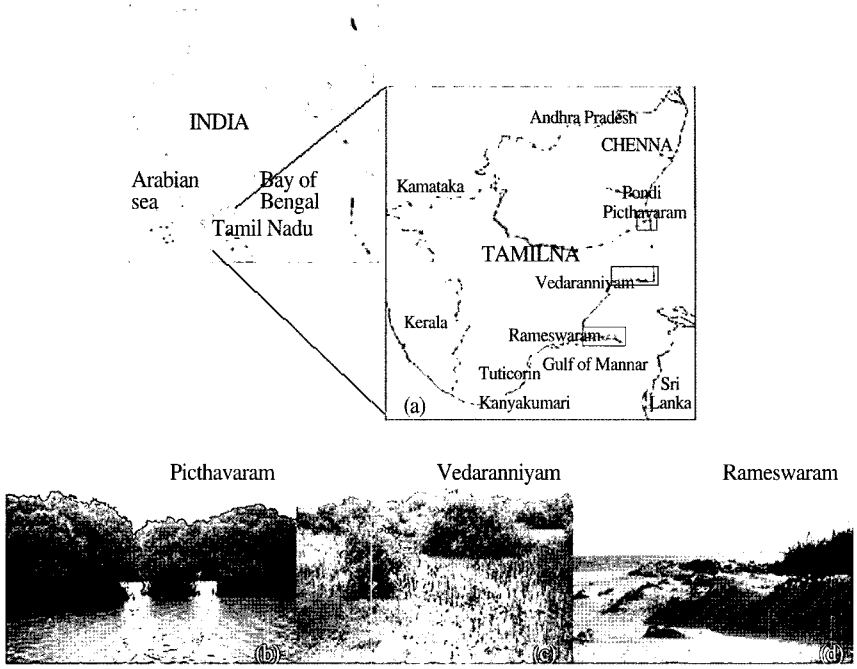

Figs. 1a-d. Location map of three coastal wetland sites of southern India (Tamil Nadu) (a), and characteristic surface cover types in the field (b-d).

delta discharge their water into these lagoons and mudflat before reaching the sea. The topography of the fringe area of the mangroves provide conditions for high frequency and extent of tidal flushing thereby creating favorable environmental conditions, particularly salinity, for the growth and regeneration of the species like Rhizophora apiculata, Rhizophora mucronata, and Suaeda maritima. The annual temperature varies between 30° to 40° C and the annual rainfall ranges from 1000 to 1500mm

In contrast, Rameswaram wetland is located within 9° 8′ to 9° 27′ N and 78° 55′ to 79° 30′ E in the southeastern part of the Vedaranniyam wetland, representative of a complex coastal sand dune ecosystem associated with the disconnected masses of huge coral reefs fringing Rameswaram and other islets in Gulf of Mannar. Human interference on deforestation and reclamation process as well as coral mining leads to the deterioration of sand dune ecosystem and environments of Rameswaram.

The primary data set consists of IRS-1C/1D LISS-III and Landsat-5 TM imageries as well as survey of India topographic maps of 1: 50, 000 scale (Table 1). Frequent and severe cloud cover did not allow the study areas to be captured by these sensors during similar periods/ seasons, and therefore images of Vedaranniyam and Rameswaram during dry season (July) and of Pitchavaram during wet season (January). Prior to the analysis, digital values recorded at the top of the atmosphere were converted to total radiance values at the satellite level and corrected for the atmospheric effects by dark-pixel substration technique (Chavez, 1988). As the radiometrically and atmospherically corrected data contained geometric errors from the sources, that range from variations in the altitude, attitude, and velocity of the sensor platform, to factors such as panoramic distortion, earth curvature, earth rotation, relief displacement, and nonlinearities in the

Table 1. Characteristics of IRS-1C/1D LISS-III and Landsat-5 TM imagery of the three wetland study sites.

Sensor	Spectral range ((m)	Resolution (m)	Date	Orbit (path/row)	Topographic map
IRS-1D LISS-3 (Pitchavaram)	0.52 - 0.59, 0.62 - 0.68, 0.77 - 0.86, 1.55 - 1.70	23.5	14-01-1998	102/65	58 M/15
IRS-1C LISS-3 (Vedaranniyam)	0.52 - 0.59, 0.62 - 0.68, 0.77 - 0.86, 1.55 - 1.70	23.5	19-07-2000	102/66	58 N/7, 58 N/11 and 58 N/15
Landsat-5 TM (Rameswaram)	0.45 - 0.52, 0.52 - 0.60, 0.63 - 0.69, 0.76 - 0.90, 1.55 - 1.75	30	12-07-1989	142/54	58 O/3, 58 O/7 and 58 O/8

sweep of a sensor's IFOV (Lillesand and Kiefer, 1994), it was necessary to georeference these images with respect to the high resolution IRS-1C panchromatic (5 m) image projected polyconically on a 1:50,000 scale topographic map as mentioned in Table 1. Adequate number of ground control points (GCPs = ((n+1) (n+2)) / 2) was selected in order to improve the georeferencing accuracy to fall within 0.3 to 0.5 pixels.

For validation of LSMM, field survey was conducted on 19 July 2000 over Vedaranniyam wetland in order to collect the ground truth data, pertaining to spectral reflectance, vegetation, soil, moisture cover fractions, from number of locations with the help of global positioning system (GPS). This was the period corresponding to the IRS-1C LISS-III overpass on this area. Canopy and soil spectroscopic measurements were collected using a handheld multispectral ground truth spectroradiometer (GTR) along the 750m mangrove-mudflat (MM) transect running from the fringe of the lagoon to mudflat areas in the western part of Vedaranniyam study site. Spectroradiometric measurements also covered areas of turbid waters, salt marsh and marsh in swamp, mangroves, and wet and dry mudflats. The total number of measurements made between 9a.m and 4p.m was 16 along this transect and 12 in the surrounding areas. Because of the inaccessibility, vegetation cover fractions in dense mangroves along the fringes of lagoon and marsh in swamps were not adequately determined with these instruments. Soil moisture and organic matter data were established from soil samples collected coincidently with the spectroradiometric measurements using laboratory methods (Bowman *et al.*, 1991; Hummel *et al.*, 2001). For the selection of training data and assessment of hard classification accuracy, a large number of ground truth data was also assimilated from other parts of Vedaranniyam and Pitchavaram wetlands before, during and after IRS IC/1D satellite overpass on these areas. For Rameswaram, field data collected from a number of points as a part of wetland monitoring program by Department of Geology and Institute of Ocean Management (IOM) at Anna University was used to assess classification accuracy of Rameswaram wetland cover features.

3. Methods

1) Traditional Hard Classification Methods

The traditional methods for inferring characteristics about the surface cover from satellite remotely sensed data are to classify each pixel into a specific land cover type based on a predefined classification scheme. These methods employ mathematical decision rules to assign image pixels to clusters representing land cover categories, in the feature space delimited by the spectral bands of the image. This study concentrated on two well-known methods: a non-parametric or unsupervised

classification based on Iterative Self-Organizing Data Analysis (ISODATA) and a parametric or supervised classification based on Maximum Likelihood Classification (MLC) method. The detailed description of these methods may be found in Shanmugam (2002).

In order to produce a single map of likeliest class, the MLC requires a number of training samples for each class. These training samples were selected from the image itself based on ground truth information. Prior to the classification, training sample signatures were evaluated to perform better classification using separability analysis by transformed divergence (TD) and Jeffries-Matusita (JM) distance measures (Swain and Davis, 1978). These are statistical measures of distance between two signatures and calculate for any combination of bands that will be used in the classification. The values of lower and upper bounds of TD and JM distance are respectively, 0 and 2000, and 0 and 1414. If the calculated divergence is equal to the upper bound then the signatures can be said to be totally separable in the bands being analyzed. A calculated divergence of zero means that the signatures are inseparable.

2) Linear Spectral Mixture Modeling (LSMM)

Spatially heterogeneous mixtures of mangrove and marsh vegetation, soil and moisture with indefinite boundaries characterize coastal wetland ecosystems of southern India. For IRS-1C/1D LISS-III and Landsat-5 TM, the instantaneous field of view (IFOV) is large enough that pixels comprise mixtures of these features. This inevitably means more cover types are included within one pixel and therefore more mixing of material spectral signatures. Sub-pixel mixing in remote sensing dictates that pixel reflectance cannot be simply interpreted in terms of properties of a single cover type. Accounting for sub-pixel variations in cover types is therefore an essential step for analyzing pixel reflectance in such heterogeneous regions (Asner and Heidebrecht, 2002). Thus, the goal of linear spectral mixture modeling (LSMM) is to estimate the fractional cover of each major landscape unit of interest within image pixels. The required inputs to LSMM are end-member reflectances that are to be unmixed. The output is a fraction image, with coefficients lying between 0 and 1 and summing to one, for each end-member along with an image containing an error of fit. These fractional images can be used to constrain additional spectral analyzes, as input to biophysical and biogeochemical models (Quarmby *et al.*, 1992; Garcio-Haro *et al.*, 1996; Asner, 1998; Asner and Lobell, 2000), or simply as a measure of land cover used to analyze spatial and temporal changes (Foody *et al.*, 1994; Roberts *et al.*, 1997; Shanmugam, 2002).

The principal assumption of LSMM is that the measured reflectance of a pixel is the linear sum of the reflectance of the mixture components that make up that pixel. It is also assumed that there is no interaction between the photons reflected by the individual pixel components. In order for the LSMM to be applied the reflectance of that pixel is assumed to be formed as the sum of the reflectance of the end member types weighted by their proportions. Mathematically, the linear spectral mixture modeling framework can be expressed as

$$R_1 = F_m R1_m + F_v R1_v + F_s R1_s + E_1 \quad (1)$$

$$R_2 = F_m R2_m + F_v R2_v + F_s R2_s + E_2 \quad (2)$$

$$R_3 = F_m R3_m + F_v R3_v + F_s R3_s + E_3 \quad (3)$$

where, R1, R2 and R3 are the calibrated signal in the respective bands 1, 2, and 3 or 2, 3, 4 of LISS-III or TM; F_m, F_v and F_s are the fraction of the pixel covered by moisture, vegetation, and soil; $R1_m$, $R2_m$, and $R3_m$, $R1_v$, $R2_v$ and $R3_v$, and $R1_s$, $R2_s$, and $R3_s$ are respective of reflectance of moisture, vegetation and soil in each of the three spectral bands. E_1, E_2, and E_3 are the error components in the respective bands of LISS-III or TM. For the sake of simplification equations (1-3) can be

written as follows

$$R_i(\lambda) = \sum_{j=1}^{n} F_j R_f(\lambda)_i + \varepsilon_i \quad (4)$$

$$0 \leq \sum_{j=1}^{0} F_j \leq 1 \quad (5)$$

where, R_i is the composite reflectance of the mixed spectrum in band i, F_j is the fraction of end-member (j) in the mixture, R_f is reflectance of that end member in band i, n is number of end members, ε is error in the sensor band i, λ is wavelength. The equation 5 constraints the fractions allowed to be between 0 and 1. Implicit in the above equations is the assumption that each cover type contributes linearly to pixel reflectance, and thus nonlinear interactions between end-members are negligible (Asner and Lobell, 2000). The schematic of LSMM is shown in Fig. 2.

The identification and selection of reflectance end-members for equation (4) can be a major problem to the accurate estimation of the sub-pixel cover fractions by LSMM. These end-members principally being pure

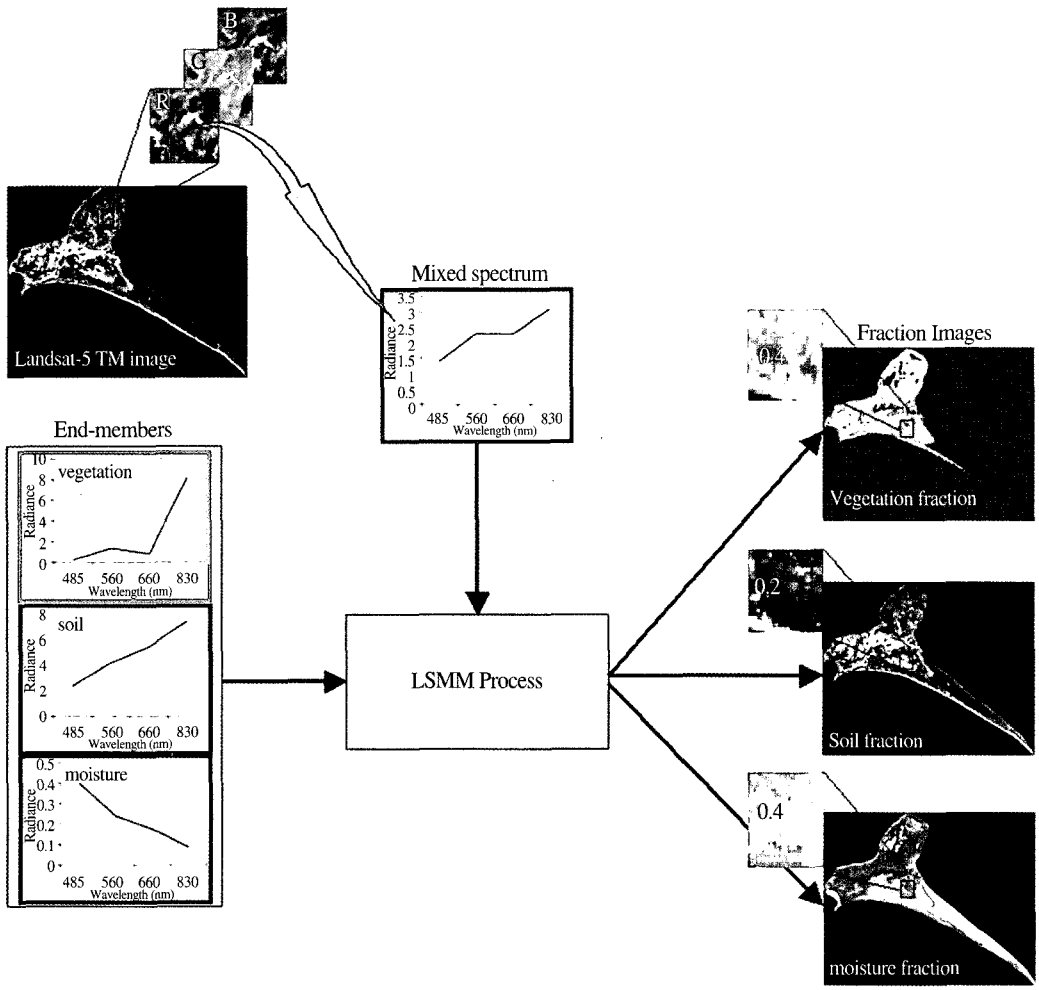

Fig. 2. Schematic of linear spectral mixture model (LSMM) showing sequence of operations carried out to derive the resultant fraction images. The observed vector is decomposed using equation 4 using spectral end-members of soil, vegetation and moisture.

reflectance spectra that are derived by a specific target material with no mixing with any other materials are usually selected either from spectral libraries built from field surveys (Asner and Heideobrecht, 2002) or from the image data (Roberts *et al.*, 1997). The use of reflectance end-members from spectral libraries is not practical because they can suffer mainly from spatial and temporal variability in reflectance properties of cover types. For instance, large differences in soil moisture over dry and wet mudflat areas or canopy senescence between the times of field spectral measurements and image acquisition can hamper interpretation of cover fraction images. It is also difficult task to obtain reference end-member spectra for all cover types, particularly in mangrove and marsh in swamp where the size of mangrove canopy in the fringes of lagoon and inaccessibility nature of swampy areas hinder the field reflectance measurements. The second approach is more realistic and derives end-member spectra directly from the image by extracting reflectance from relatively pure pixels. There are different methods for selecting spectral end-members from the image, including principal component analysis (PCA), pixel purity index (PPI) and minimum noise fraction (MNF). This study uses spectral end-members identified from the feature space of red and near-infrared (NIR) bands and of MNF bands of LISS-III and TM images. The image-based end-members are ideal because they are drawn from the population of data points to be analyzed in the same scale of measurement (Roberts *et al.*, 1997). More about selection of end-members using different methods can be found in Shanmugam (2002).

4. Results

1) Traditional Hard Classification Methods

ISODATA classification performed on LISS-III and TM images of the three study sites produced broad wetland cover map for 5, 10, 15 and 20 classes. The purpose of deriving maps with increased number of classes is to assess the performance of ISODATA classification and rate of classification accuracy from lower number classes to higher number of classes. The derived classes were assigned and labeled to actual class based on the knowledge of study area, topographic and existing coastal ground truth maps. Comparing to manual delineations from the imagery (hard copy), this automated method produced maps with more details of the available wetland cover types (not shown). The accuracy of these classifications was then assessed because there is more of a need to assess the reliability of the results in such a complexity of digital classification. Thus, the reporting and evaluation of the comparison of the classified data to verification data included the generation of an error matrix and statistical evaluation of that matrix. The error matrix provided a concise means of examining per class map errors by including both errors of commission and errors of omission (Dicks and Lo, 1990; Congalton, 1991). The accuracy assessment of the ISODATA classification using error matrix was carried out on threshold images of 5, 10, 15 and 20 classes by two statistical techniques the overall accuracy and KAPPA accuracy. The first one is the simplest descriptive statistic technique which computes accuracy by dividing the total correct (i.e., the sum of the major diagonal) by the total number of pixels in the error matrix, while KAPPA accuracy is the discrete multivariate technique in which a KHAT statistic is used as a measure of agreement or accuracy. The KHAT statistic is computed as

$$K = \frac{N\sum_{i=1}^{r} x_{ii} - \sum_{i=1}^{r}(x_{i+} * x_{+i})}{N^2 - \sum_{i=1}^{r}(x_{i+} * x_{+i})} \quad (6)$$

where r is the number of rows in the matrix, x_{ii} is the

number observations in row i and column i, x_{i+} and x_{+i} are the marginal totals of row i and column i, respectively, and N is the total number of observations.

Overall accuracy and KAPPA accuracy were computed and compared for all class types (Figs. 3a and b). It was observed that the overall accuracy obtained for Pitchawaram was 84%, 79%, 78% and 76.5% for 5, 10, 15 and 20 classes respectively. The KAPPA accuracy was 0.78, 0.74, 0.70, and 0.68 for 5, 10, 15 and 20 class types respectively. Overall accuracy and KAPPA accuracy progressively decreased when more number of information classes were subjected to be derived. The progressive decrease in classification accuracy towards increased number of classes is thought to result essentially from spectral confusion/overlapping between the following classes: mangrove and non-mangrove vegetation, degraded mangrove and marsh in swampy areas, marsh and degraded mangrove, marsh and mudflat, mudflat and fallow and lagoon and inland waters. Similar trend was seen in Vedaranniyam study site but with slightly improved accuracy associated with these four classifications (Figs. 3a and b). Overall accuracy was observed to be respective of 86%, 74%, 66.6% and 60.5% for 5, 10, 15 and 20 classes, while KAPPA accuracy respective of 0.80, 0.67, 0.59, and 0.56 for 5, 10, 15 and 20 classes. Misclassification occurred primarily in mangrove and agricultural plantation, mangrove and scrub, marsh in swamp and wet mudflat as well as within marsh communities, dry mudflat and reclaimed mudflat, mudflat and fallow, wet mudflat and saltpan, and sandy areas and dry mudflat. In contrast with previous cases, ISODATA algorithm applied on relatively low spatial resolution TM imagery resulted in maps of 5, 10, 15 and 20 classes with improved accuracy, indicative of spatially simple and well distinct cover types associated with Rameswaram sand dune ecosystem. It showed overall accuracy of 94%, 91.5%, 89.7% and 88.5% for the respective of 5, 10, 15 and 20 classes. A similar tendency in decrease of classification accuracy was found in KAPPA accuracy that yielded 0.86, 0.80, 0.76, and 0.74 for the above class types, corroborating the fact that spectral confusion and potentially mixed pixels are the principal factors of the decreased accuracy, particularly for more number of classes derived from LISS-III and TM.

With the aim of deriving classes with improved accuracy, supervised classification using MLC was applied to classify the LISS-III and TM imagery into 5, 10, 15 and 20 classes. The main purpose of attempting MLC among other classification algorithms was that it has been proven to be the one that obtains the best results for classification of remotely sensed natural resource data (Mather, 1987; Shettigara, 1991). Unlike the automated ISODATA classifier, MLC classification

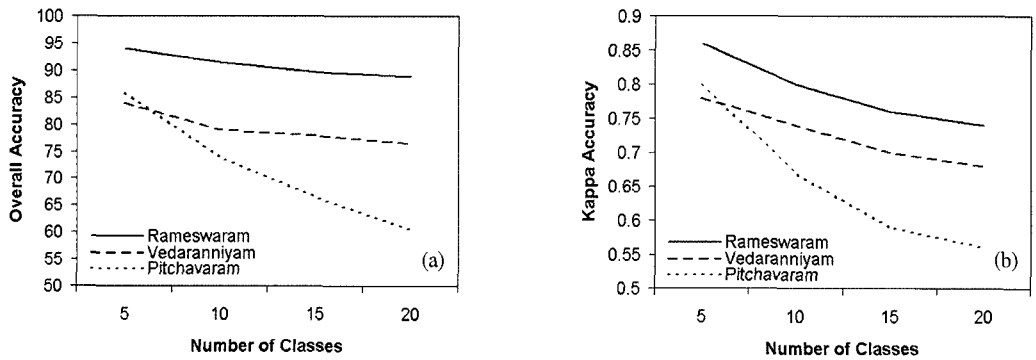

Figs. 3a and b. Overall accuracy and KAPPA accuracy for maps of 5, 10, 15 and 20 classes derived from LISS-III and TM image data of the three study sites by ISODATA algorithm.

started with a number of training samples, which resulted in various signatures, and followed by class assignment using decision rule. The ground truth maps combined with field knowledge and unsupervised classification results were the basis for selecting accurate and reliable training samples for performing MLC classification. Before performing the MLC classification, the signatures of these training samples were evaluated by using TD and JM distance statistical measures applied on three bands LISS-III and five bands TM image data. Separability analysis indicted that the selected training sample signatures were appreciably separable but with a tendency of seemingly decreased overall minimum separability when number of sample signatures increased (Figs. 4a-c). The poor separability for more number of class signatures was noticeable in all study sites, resulting mainly from spectral similarity/ overlapping among certain wetland categories mentioned earlier. However, Rameswaram study site contrasting with Pitchawaram and Vedaranniyam yielded relatively high separability for all training sample signatures. Following the performance of separability analysis, the wetland information classes were derived from LISS-III and TM images of these three study sites (shown in Figs. 5a-l) and the accuracy of these classes was assessed by using overall accuracy and KAPPA accuracy (using equation 6). Note that sub-classes obtained are based on density, and wetness and dryness in the case of marsh, scrub, mudflat, fallow and sandy area classes and level of turbidity in the case of water class.

Figs. 6a and b compare the overall and KAPPA accuracy for derived wetland classes of the three study sites by MLC. Overall accuracy in Pitchawaram seemed

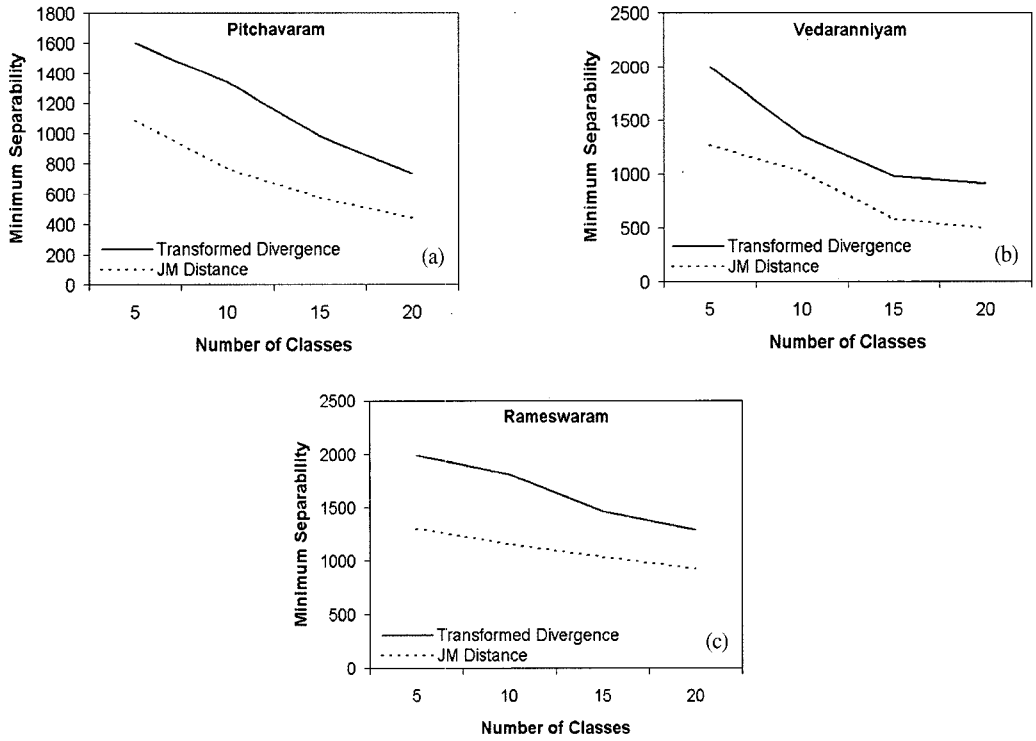

Figs. 4a-c. Overall minimum separability computed for 5, 10, 15 and 20 training samples from LISS-III and TM image data of three study sites using Transformed Divergence (TD) and Jeffries-Matusita (JM) distance measures.

Figs. 5a-l. Maps of 5, 10, 15 and 20 classes derived from LISS-III and TM image data of three study sites by maximum likelihood classification (MLC) method. Because of the class inseparability, only 18 classes were extracted for Rameswaram study site.

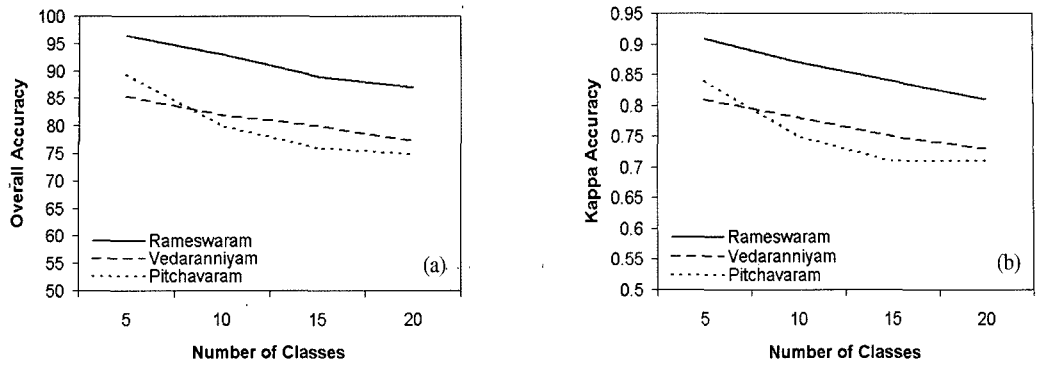

Figs. 6a and b. Overall accuracy and KAPPA accuracy for maps of 5, 10, 15 and 20 classes derived from LISS-III and TM image data of the three study sites by MLC algorithm.

to be 84%, 79%, 78% and 76.5% for 5, 10, 15 and 20 classes respectively, while KAPPA accuracy was 0.78, 0.74, 0.70, and 0.68 for 5, 10, 15 and 20 classes respectively. In Vedaranniyam, a fairly improved overall accuracy for 5, 10, 15 and 20 classes achieved was 86%, 74%, 66.6% and 60.5% respectively. KAPPA accuracy for these class types was 0.80, 0.67, 0.59 and 0.56 respectively. Rameswaram contrasts with these two sites in improving overall accuracy and KAPPA accuracy from 94%~88.5% and 0.86~0.74 for the obtained class types. It should be noted that although MLC improved classification accuracy over ISODATA classification, overall and KAPPA accuracy remained diminished when more number of wetland classes were subjected to be extracted from LISS-III and TM image data. Perhaps this is related to occurrence of number of misclassified pixels, particularly in areas of mangrove and non-mangrove vegetation, degraded mangrove and marsh in swamp, marsh and mudflat, mudflat and fallow, aquaculture ponds and fallow or mudflat, agricultural plantation and scrub, sand dunes and fallow, and between coral reefs (Rameswaram). The misclassification of these pixels could be elucidated by number of factors, such as spectral confusion/overlapping, size and inhomogeneity of training samples (each training sample perhaps contains certain proportion of soil, vegetation or water), and spectral mixtures within the image pixels. Shanmugam (2002) found that statistical characterization of the above classes used in MLC was not sufficient to separate from the inadequate IFOV of the LISS-III and TM, which caused the geographical area subtended by a pixel to contain a mixture of land cover types. To overcome these problems, a soft classification based on linear spectral mixture modeling was performed, evaluated and compared with the traditional hard classification methods that labeled the entire pixel as belonging to one class.

2) Linear Spectral Mixture Modeling (LSMM)

In order to successfully apply the LSMM, it was very essential to accurately estimate the spectral end-members for each component of soil, vegetation and moisture. These end-members were determined from the image through two approaches, based on two-dimensional scatter plot of red and NIR bands, and MNF transformation. This study did not use the field-derived reflectance end-members because they were not adequate to be used in LSMM and covered only a small range of cover types actually present in the study site. Furthermore, the reference end-members from the field can suffer from temporal variability in reflectance properties of cover types, causing some error in estimating the proportions of each cover types in the

sub-pixel classification analysis (Asner and Heidebrecht, 2002). Fig. 7a allows the identification of three dominant spectral end-members, soil, vegetation and moisture, at the extremes of image feature space of red (LISS-III B2) and NIR (LISS-III B3) bands. These end-members were assumed to represent the purest pixels in the LISS-III image. An average of 3-7 pixels of these vertices were calculated and used in LSMM. Cautions needed to be taken to identify outliers when selecting these end-members. The Vedranniyam image contrasted with Pitchavaram image because the scatter plot of LISS-III B2 and B3 showed rather asymmetrical patterns in pixel distributions not allowing the selection of appropriate spectral end-members from the LISS-III image. Thus, this study needed for MNF transformation that, applied on LISS-III image data, produced bands represented by coherent images. The MNF transform is one of the often-used methods for reducing redundancy of information between image bands and assisting selection of accurate and reliable end-members (Rainey *et al.*, 2003). The spectral end-members were derived from the scatter plot of MNF B1 and MNF B2 shown in Fig. 7b. The selection of first two coherent MNF bands was that they were found to contain 96% of the total statistical variance in LISS-III image data set. The moisture end-member was identified at the top left vertex while vegetation end-member on the right vertex of the MNF scatter plot. The soil end-member was selected from the pixels at the lower right vertex of the MNF scatter plot (Fig. 7b).

The primary results of LSMM were separate images for each of the end-members (soil, vegetation and moisture) containing an estimate of the fraction of that end-member in each pixel. Assuming the LSMM and that the spectral signatures of end-members could be derived from the scatter plots (Figs. 7a and b), the three fraction images provided information on the abundance of particular wetland cover type in each pixel of the LISS-III and TM image. Figs. 8a-c and Fig. 2 illustrate the fraction characteristics of the available wetland cover classes in three study sites. In the fraction images, each pixel value corresponds to the fraction of soil, vegetation and moisture in that pixel and the range of fraction values is between 0 and 1. Pixels with higher abundance of the end-member appear to be brighter in the corresponding fraction image. In the soil fraction, mudflat and sandy areas have significantly higher values (0.50~0.70%), while mangroves and marsh have very low fractions values (darker tone). In the vegetation fraction, moisture and mudflat and bare soils represented

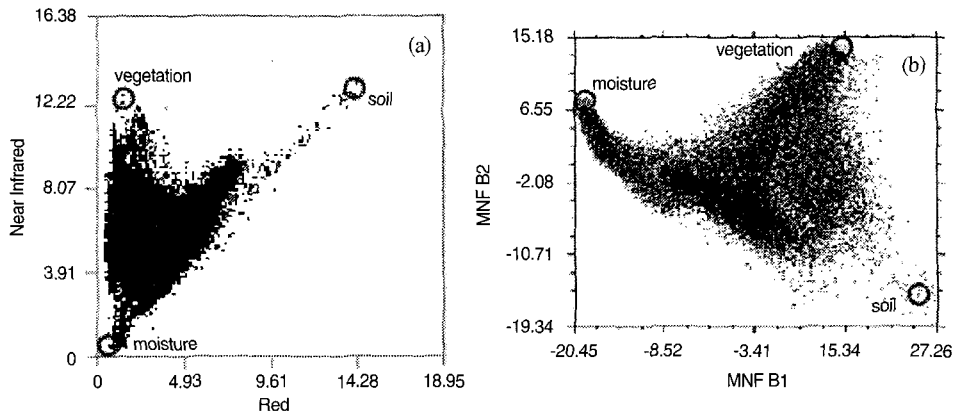

Figs. 7a and b. Identification of spectral end-members from the feature space of red and NIR bands and of MNF B1 and B2 of LISS-III image data in Pitchavaram and Vedaranniyam study sites.

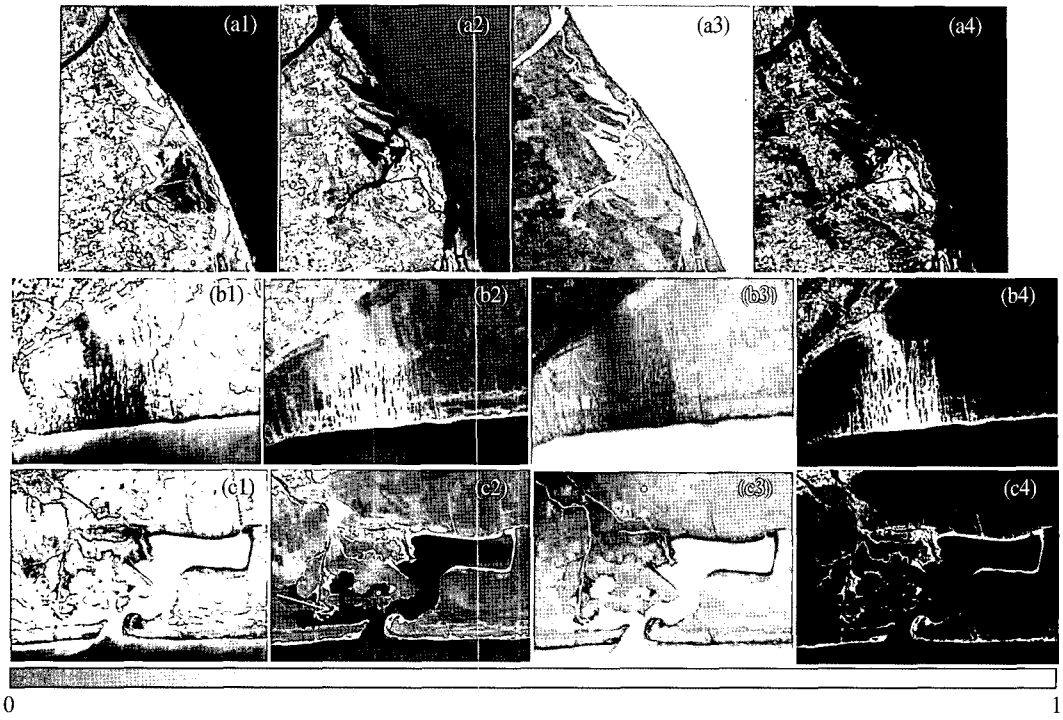

Figs. 8a-c. Fraction images of the three end-members, soil (a1, b1 and c1), vegetation (a2, b2 and c2), and moisture (a3, b3 and c3), obtained by LSMM of LISS-III images of Pitchavaram (a) and Vedaranniyam (b and c) study sites. The accompanying errors (not included) for these fractions ranged from 1.2~2 in Pitchavaram, 1~1.7 in Vedaranniyam and 0.8~1.9 in Rameswaram. For validation, the NDVI image was derived and shown in Figs. 8a4, b4 and c4. In soil fraction images, the brighter areas indicate sand and dry mudflat abundances, while grey tone represents wet mudflat/swampy areas and turbid waters. In vegetation fraction images, the brighter areas indicate dense and sparse mangroves abundances while grey tone indicative of marsh and fallow lands. In moisture fraction images, water appears to be brighter and wet mudflat is indicated by dull grey tone. NDVI images show apparent patterns of mangroves and marsh vegetation in Pitchavaram and Vedaranniyam study sites. Fraction images for Rameswaram study site are shown in Fig. 2.

by murky tone have the low fraction values (<0.20%). It appeared to be large variations between the fraction values of mangrove (0.62~0.75%) and marsh (0.40~0.55%) and marsh in swamp (0.23~0.40%), resulting from crown characteristics (density, leaf area index, tallness, etc) and possibly reflectance properties of the background cover types. Overall, marsh vegetation (grey tone) has lower fraction values than mangrove and other forest plantations. In the moisture fraction, moisture has the highest value (brighter tone) and vegetation and sandy areas the lowest values (represented by darker tine). Mudflats have some fraction values of moisture (0.20~0.35%) than sandy areas (<0.15%). The associated error fraction indicated that high quality fraction images were obtained and the results were reliable because the error value for all wetland cover types was very small (less than 0.03%). It is evident that the LSMM results were beneficial in the sense that the method recognized the fact that image pixels typically contained components of wetland cover types and provided a more accurate representation of the soil, vegetation and moisture cover present in the three

study sites.

This study assessed the reliability of the LSMM results by comparing model-derived fraction estimates with field-derived fractional cover estimates as well as image-derived quantities. In order to compare the fraction estimates of each continuous field (end-member) from each of the three study sites, the first step involved converting the output from the LSMM to the percent covers of the different end-members. However, the fractional files contained the estimates of the fractional coverage associated with each end-member and the values between 0 and 1 could be interpreted as percentages for that particular end-member. The fraction values varied directly with proportional land cover (i.e., 0-100). Firstly, the LSMM results were compared with normalized difference vegetation indices (NDVI) and with field data collected from the Vedaranniyam study site. Many studies have attempted to correlate vegetation indices (NDVI) to the fractional coverage of vegetation and soil (e.g. Carlson and Ripley, 1997; Shanmugam, 2002) because NDVI is an indicator sensitive to chlorophyll activity and to the density of vegetation cover (Duncan *et al.*, 1993). This vegetation index was formulated to substract the effect of reflectance in the red band from NIR reflectance (NDVI = (NIR-Red)/ (NIR+Red). The NDVI value in a given pixel ranges between 0 and 1 where 0 represents 0% vegetation, while 1 represents 100% vegetation in that pixel. Therefore, a vegetated surface yielded high values because of their high NIR reflectance and low red reflectance (see Fig. 12b), bare soil and sandy areas resulted in values closer to 0 due to nearly similar reflectance in the two bands, water having larger red reflectance than NIR yielded some time negative values. The change in NDVI values in vegetative areas depends on their phonological cycle (Figs. 8a4, b4 and c4).

Fig. 9a shows the correlation between the proportion of vegetation fractions derived from LSMM and NDVI in three study sites. It appears that vegetation fraction values increase with increasing NDVI values. It exhibits a positive correlation between vegetation fraction with NDVI, with the squared correlation coefficient (r^2) respective of 0.92, 0.95 and 0.96 for Pitchavaram, Vedaranniyam and Rameswaram. These values are higher than that (r^2 = 0.602) reported by McGwire *et al* (2000) when correlating NDVI with % green cover for Providence Bajadas area, California using hyperspectral image data. The highly heterogeneous and complex

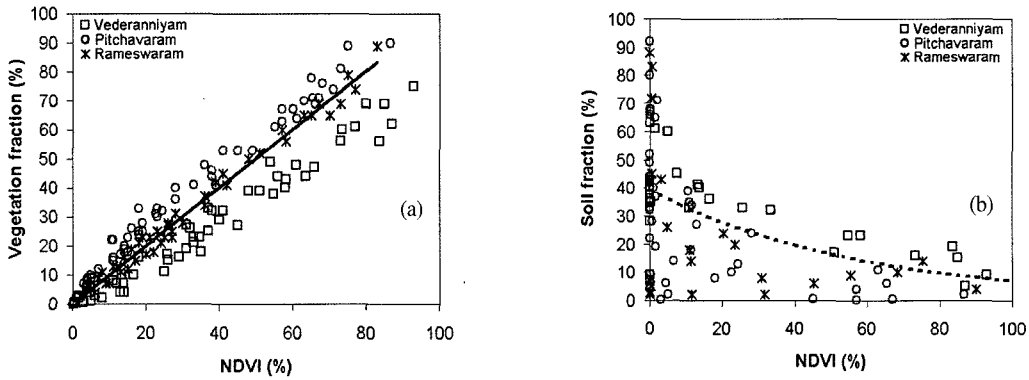

Figs. 9a and b. Validation of LSMM results in the three wetland study sites. (a) Vegetation fraction correlates very well with NDVI fractions (r^2 = 0.92 in Pichavaram; r^2 = 0.95 in Vedaranniyam; r^2 = 0.96 in Rameswaram). (b) Soil fraction correlates poorly with NDVI (i.e., r^2 = 0.13 in Pitchavaram; r^2 = 0.39 in Vedaranniyam; r^2 = 0.53 in Rameswaram).

nature of Pitchavaram mangroves and marsh, associated with Vellar-Coleroon estuarine complex, resulted in relatively poor correlation between NDVI and vegetation fraction than Vedaranniyan wetland site. The highly dispersed marsh vegetation in Vedaranniyam mudflats underestimated the vegetation fraction in LISS-III image and resulted in poor correlation between vegetation fraction and NDVI than Rameswaram site, where the vegetation fraction from LSMM tended to have one-to-one correlation with NDVI owing to distinct patches of cover types. While NDVI is correlated with the vegetation fraction, considerable scatter is present in each of the three study sites due to variable background reflectance (i.e., soil and moisture) and differences in the structure of the vegetation canopies between plots. In contrast, Fig. 9b shows the negative relation between NDVI and soil fraction estimates for all three study sites. The r^2 for the NDVI and soil fraction relation was 0.13, 0.39 and 0.53 for Pitchavaram, Vedaranniyam and Rameswaram respectively. A positive relationship between NDVI and the vegetation fraction, and a negative relationship between NDVI and the soil fraction indicate the correctness of the LSMM and the reliability of the derived sub-pixel proportions of vegetation and soil.

The soil and moisture fraction images derived from LSMM were also compared with field data collected from the discrete locations around Muthupet mudflat and lagoonal areas in the western part of the Vedaranniyam study site. Fig. 10a shows the relationship between actual moisture fraction in the field and computed moisture fraction by LSMM. It appears that the computed moisture fractions by LSMM were substantially overestimated by about 10-24% at first 7 stations (excluding 4 and 5), while it was nearly consistent with the actual moisture fraction, with an overestimation by about 5-10% at the remaining stations. This overestimation occurred due to the significantly large IFOV of the sensor covering a highly varied surface moisture cover at these stations. However, overall accuracy of LSMM for the estimates of moisture fraction was found to be 92%. In contrast, the soil fractions estimated by LSMM appeared to be lower by about 10~32% than the actual soil fractions from the field (Fig. 10b). When the actual soil fraction did not account for the imperceptible surface green matter in the field, the presence of microphytobenthos attenuated the spectral signal of the mud resulting in underestimation of soil abundance at all stations, where the vegetation abundance increased by about 10~25%. Examination of the associated error image revealed that the LSMM error increased to about 2% in the fine-

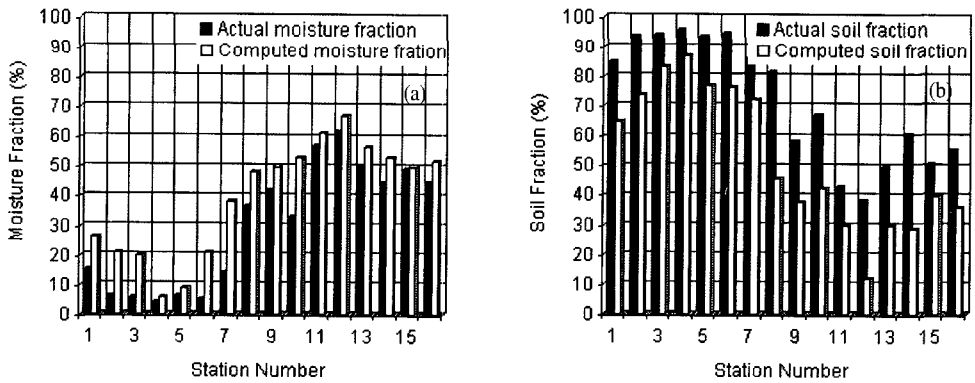

Figs. 10a and b. Comparison of actual and computed fractions of moisture and soil end-members in Vedaranniyam study site. Soil moisture was determined at 16 discrete locations in the western part of Vedaranniyam wetland.

grained mudflat areas, which were covered by microphytobenthos. The overall accuracy can be said to be about 96% for the estimates of soil fraction by LSMM.

3) Comparison of the Results of LSMM and MLC Classification

In order to make results of per-pixel classification (MLC) comparable to the LSMM qualitatively and quantitatively, the areas of different wetland classes depicted from MLC were used in LSMM to derive fraction images of soil, vegetation, moisture and accompanying error for each class. The means of these fractions computed were taken to explain the difference between the results of per-pixel and sub-pixel classifications. Fig. 11 gives an example illustrating the mean fraction characteristics of some typical wetland classes derived from per-pixel classification (MLC) in the Pitchavaram study site. It is apparent that the dense mangrove (DM) class consisted of 68.5% vegetation, 16% soil, 14% moisture and 1.4% error, while degraded mangrove (DGM) class embraced 45% moisture, 28% soil, 25% vegetation and 2% error. Similarly, marsh vegetation class depicted from MLC is shown to contain 47% vegetation, 33% soil, 18% moisture and 2% error. In wet mudflat (WMF) class, 47% soil, 37% moisture, 15% vegetation and 1% error could constitute the WM class, while 70% soil, 18.8% moisture, 10% vegetation and 1.2% error accompanied with the dry mudflat class (DMF) depicted from MLC classification. The associated error fractions demonstrate that the error was significantly low for all class types, but slightly high errors for degraded mangrove and marsh classes, which underlie the fact that simplifying assumptions were made to the end-member extraction and to the LSMM algorithm due to the spectral limitation of the sensor and to ease the procedure could elucidate part of such high errors and variations in the error fractions obtained for these class types.

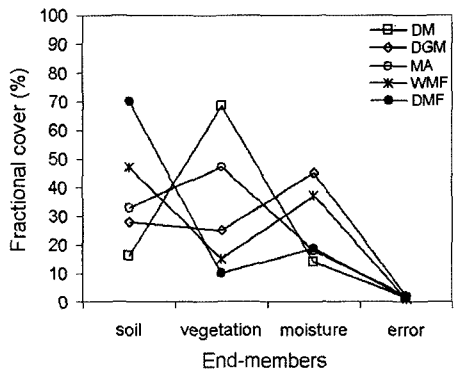

Fig. 11. Mean fractional cover percentage obtained from LSMM for different wetland cover types derived from MLC algorithm using LISS-III image data of Pitchavaram study site. DM - dense mangrove, DGM - degraded mangrove, MA - marsh, WMF - wet mudflat, DMF - dry mudflat.

On the other hand, a 750 m transect was established in the western part of Vedaranniyam wetland (Muthupet), running from the fringes of the lagoon (where high density of mangroves could be observed) to mudflat. This transect location is indicated by an arrow in Fig. 8c2 and transect is referred to as mangrove-mudflat (MM) transect. Several measurements were made along this transect, coinciding with the flood tide and LISS-III over pass on 19-07-2000. The sparse mangrove areas just behind the dense mangroves on the fringes of lagoon were partially covered by turbid waters of the flood tides. The reflectance properties of lagoon waters, dense and sparse mangroves and bare soils on the mudflat were measured at number of stations along the MM transect, using a field ground truth spectroradiometer (GTR). The GTR collected upwelling radiance measurements in the spectral range corresponding to TM bands (first four bands) were converted to reflectance using a spectralon calibration panel. In order to compare the field measurements with LSMM, the reflectance values were converted to percentile reflectance. Fig. 12a displays turbid water

spectra collected from the lagoon beside the start of the MM transect, indicating that the reflectance percentage at GTR B2 increases with increasing suspended sediment (SS) concentrations 14~58 g/m^3. Because of the high SS concentration (58 g/m^3) in shallow waters occupying sparse mangroves, the GTR reflectance notably increased at all bands compared to lagoon water reflectances (top spectrum in Fig. 12a). Fig. 12b shows field spectra collected over dense and sparse mangroves and marsh vegetation. Note that the reflectance percentage at GTR B4 (corresponding to TM B4) progressively increased from sparse to dense mangroves. The sparse mangroves have low reflectance percentile values due to canopy structure (with relatively low pigment composition and leaf area index) associated with turbid waters. Similarly, reflectance spectra measured in wet and dry mudflats are shown in Fig. 12c, where the reflectance percentile values appear to have increased with increasing wavelength (GTR bands) and decreasing organic matter and moisture content. These two parameters together with surface sediment properties determine the surface reflectance characteristics of mudflats (Thomson *et al.*, 1998; Rainey *et al.*, 2003). Consistent with previous studies,

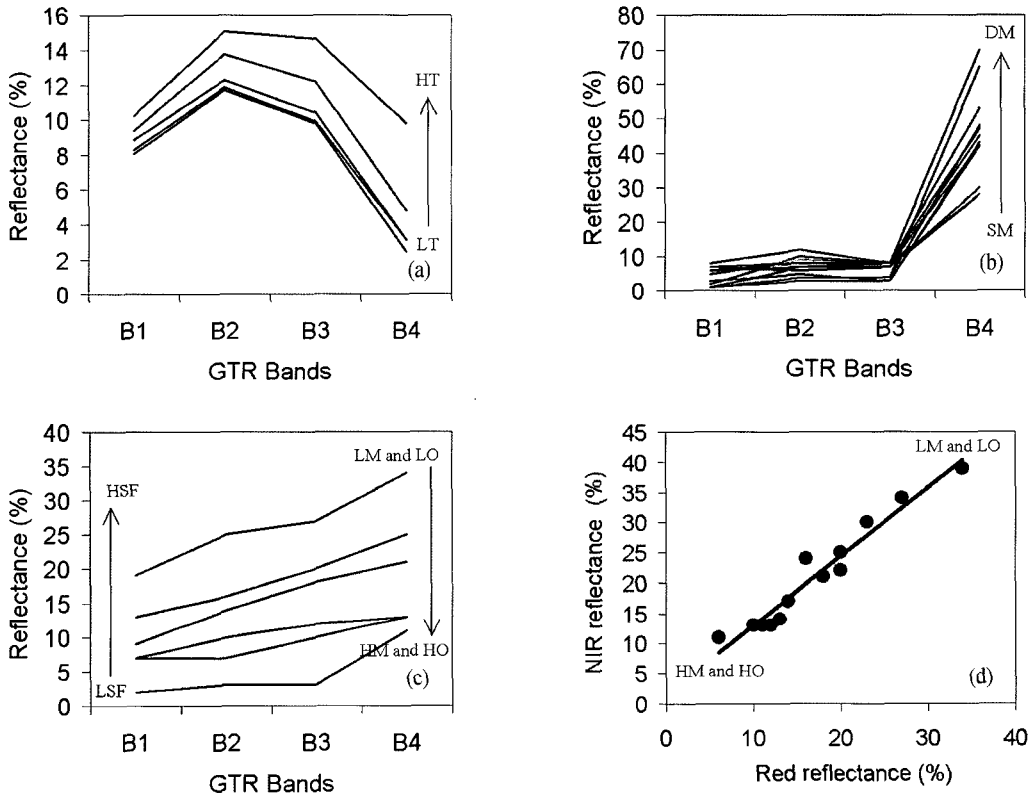

Figs. 12a-d. Field reflectance spectra of turbid waters, mangroves and soils (mudflat) measured with GTR instrument along the 750 m mangrove-mudflat transect (indicated by an arrow in Fig. 8c2) in the western part of Vedaranniyam wetland. LT - low turbid, HT - high turbid, SM - sparse mangrove, DM - dense mangrove, HM - high moisture, HO - high organic matter, LM - low moisture, LO - low organic matter, LSF - low soil fraction, HSF - high soil fraction. SS concentration determined was 14 ~ 58 g/m^3 (a), while the determined moisture content and organic matter varied from 5.4% ~ 53.5% and 0.2% ~ 4.3% respectively (c and d). The actual soil fraction ranged from 17% ~ 69% (c).

the scatter plot of GTR B3 (red) and GTR B4 (NIR) in Fig. 12d demonstrates a good linear relationship between these two bands reflectance properties, which increased monotonically with decreasing organic matter (0.2~4.3) and moisture content (5.4~53.5) determined in the field.

Fig. 13 compares the results of LSMM with MLC on LISS-III image data along the 750 m mangrove-mudflat (MM) transect in the western part of Vedaranniyam study site. The horizontal profile reveals that MLC produced a single map containing broad wetland cover types that included dense and sparse mangroves and mudflat along the 750 m MM transect area, while the LSMM was able to generate more accurate areal estimates of the end-end-member classes along this transect, matching closer to the field estimates as shown in Figs. 12a-c. Unlike MLC, the LSMM did not rely on the identification of pixel clusters with similar reflectance spectra, but rather it was able to consider each pixel individually and assessed the presence and proportion of selected end-members. The vegetation fraction produced by LSMM demonstrates that the sub-pixel dense mangrove cover ranged from 55~87% within the 200 m MM transect area, followed by a dramatic decrease in vegetation fraction representing 20~55% of sparse mangroves standing in turbid water of flood tides between 200 and 500 m transect area. Attenuation by both sparse mangroves and turbid waters governed the spectral reflectance characteristics of this region (Figs. 12a and b). The vegetation fraction further decreased by about 20~3% towards mudflats that were covered partly by the patches of microphytobenthos. On the contrary, soil abundance was significantly low (6~34%) within 375m MM transect area (where the dense and sparse mangrove areas appeared to diminish the proportional soil cover) and increased rapidly by about 34~78% towards mudflat that attenuated grater than other cover types. The estimates of these two fractional cover could determine the moisture fraction that was substantially low in both dense mangroves and mudflat areas, but tending to increase by about 23~47% in the sparse mangrove areas covered with turbid waters. The error fraction along this transect appeared to be significantly less than 2%. The comparative results indicate the efficiency of the recently evolved LSMM method that proved to maintain higher accuracy in classification and provided a more realistic representation of the coastal wetland landscape as it estimated continuous fields of wetland cover, as opposed to the patchy and discrete nature of traditional per-pixel classification techniques.

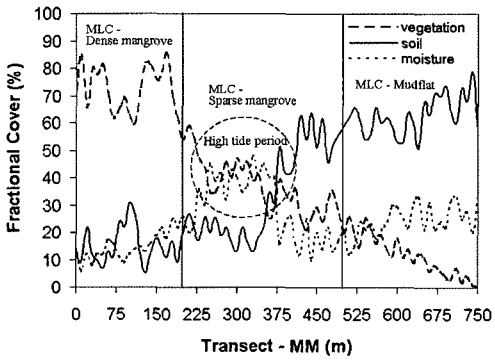

Fig. 13. Comparison of the results from LSMM and MLC applied to LISS-III image data along the 750 m mangrove-mudflat (MM) transect, which runs from the fringes of the mangrove to mudflats near Muthupet lagoon in the western part of Vedaranniyam study site.

5. Discussion and Conclusions

Coastal wetland mapping and monitoring is crucial for preserving valuable wetland ecosystems. Thus, the development of remote sensing techniques for wetland monitoring is urgent. A special emphasis in this study was placed on the analysis of IRS 1C/1D LISS-III and Landsat-5 TM imageries, because they are higher resolution data and the most commonly used imageries when referring to previous studies that employed

classification and sub-pixel mixture analysis (Andrew, 2000; Shanmugam, 2002). This study compared the LSMM with traditional hard classification methods such as ISODATA and MLC algorithms applied to IRS-1C/1D LISS-III and Landsat-5 TM image data in three different coastal wetland sites of southern India. The result showed that ISODATA and MLC algorithms provided summary information about various coastal wetland features in a relatively quick manner and seemed to be well suited to map wetland cover types in an efficient manner compared to the manual delineation technique using FCC image. However, the accuracy analysis based on overall and KAPPA accuracy measures suggested that classification accuracy appeared to be progressively decreased when more number of classes were subjected to be derived from LISS-III and TM image data by ISODATA and MLC algorithms, although dominant cover types (few classes) in each pixel were easily identified without the classification being overly hard. In real situations, it was not often that such pixels contained just one dominant class. To handle sub-pixel mixture problems, LSMM was therefore used to determine proportional estimates of wetland cover in each pixel of the imagery.

The LSMM is a physically-based image analysis model that supports repeatable and accurate extraction of quantitative sub-pixel information. The main advantage of application of this model is that wetland cover types occupying from a whole to a small fraction of an image pixel could be detected. Unlike supervised and unsupervised image classifications based on MLC and ISODATA, the LSMM did not rely on the detection or identification of pixel clusters with similar reflectance spectra. Rather, it was able to consider each pixel individually and assess the presence and proportion of select end-members. LSMM produced fraction images that were pixel-by-pixel measures of the percent composition for each end-member in the linear spectral mixture modeling. Fraction images produced with LSMM appeared to be an effective means of mapping mangrove and marsh vegetation and other associated wetland cover types in such highly fragile ecosystems. The findings showed that the LSMM was able to generate more accurate areal estimates of the end-member classes, matching closer to the field data estimates. Since supervised and unsupervised methods were based on predefined classification schemes, classifying entire pixels often produced too high or low estimates of wetland cover classes due to the inability to distinguish sub-pixel covers. In contrast, the LSMM proved to maintain higher accuracy in classification and provided a more realistic representation of the landscape as it estimated continuous fields of wetland cover, as opposed to the patchy and discrete nature of traditional per-pixel classification techniques.

Results compliment the finding of a small number of previous studies, that support the use of LSMM in characterizing coastal wetland cover composition and areal estimates, due to its ability to produce fractions representative of sub-pixel components directly related to wetland cover types and relative area. Higher accuracy in estimating wetland composition and proportional cover provided higher quality data for use in other application studies and input into biophysical, biogeochemical and other ecosystem models. Although the application of the LSMM offers the advantages of simplicity and ability to apply the model over large areas using reference reflectance end-members data, the model might also make overly simplified assumptions. For example, in LSMM, a pixel is represented by two or more cover types that occur in patches that large relative to the sensor's IFOV and it is assumed that proportions of the end-members can be estimated because mixing occurs in a linear manner. However, linear mixing does not apply to cases where the composite occurs at a scale that is fine relative to the IFOV of the sensor (Zhu and Evans, 1994). Since, mixing would occur before radiation reaches the sensor, the components of the

composite would not be able to be estimated using the LSMM approach described in the previous section. However, it should be noted that nonlinear mixing is likely only to occur when component surfaces arise in highly dispersed patterns. Owing to the nature of the wetland and scene characteristics, the LSMM has been judged to be adequate for this purpose of the study.

Acknowledgements

This research was supported in part by the Department of Geology, Anna University, Chennai, India. The author would like to thank Dr. R. Krishnamoorthy, Lecturer, Department of Applied Geology, University of Madras for having provided some filed instruments for this study. A part of this research work was also supported by KORDI under the contract PN 541-00

References

Andrew J., F. John., J. Sara, and B. David, 2000. Quantifying vegetation change in semiarid environments: Precision and accuracy of Spectral Mixture Modeling and the Normalised Difference Vegetation Index. *Remote Sensing of Environment*, 73: 87-102.

Asner, G. P., 1998. Biophysical and biogeochemical sources of variability in canopy reflectance. *Remote Sensing of Environment*, 64: 234-253.

Asner P. and B. Lobell, 2000. A biogeophysical approach for automated SWIR unmixing of soils and vegetation. *Remote Sensing of Environment*, 74: 99-112.

Asner, G. P. and K. B. Heidebrecht, 2002. Spectral unmixing of vegetation, soil and dry carbon cover in arid regions. *International Journal of Remote Sensing*, 23(19): 3939-3958.

Bastin L., 1997. Comparison of fuzzy c-means classification, Linear mixture modelling and MLC probabilities as tool for unmixing coarse pixels. *International Journal of Remote Sensing*, 18(17): 3629-3648.

Bolstad, P. V. and T. M. Lillesand, 1991. Rapid maximum likelihood classification. *Photogrammetric Engineering and Remote Sensing*, 57: 67-74.

Bowman, R. A., W. D. Guenzi, and D. J. Savory, 1991. Spectroscopic method for estimation of soil organic carbon. *Soil Science Society of America Journal*, 55: 563-566.

Carlson, T. N. and D. A. Ripley, 1997. On the relationship between NDVI, fractional vegetation cover, and leaf area index. *Remote Sensing of Environment*, 62: 241-252.

Chavez, P. S., 1988. An improved dark-object subtraction technique for atmospheric scattering correction of multispectral data. *Remote Sensing of Environment*, 24: 459-479.

Cochrane, M. A. and C. M. Souza, 1998. Linear mixture model classification of burned forests in the eastern Amazon. *International Journal of Remote Sensing*, 19: 3433-3440.

Congalton, G., 1991. A review of assessing the accuracy of classifications of remotely sensed data. *Remote Sensing of Environment*, 37: 35-46.

Dicks E. and H. C. Lo, 1990. Evaluation of thematic map accuracy in a land-use and land-cover mapping program. *Photogrammetric Engineering and Remote Sensing*, 56(9): 1247-1252.

Duncan, J., D. Stow., J. Franklin, and A. Hope, 1993. Assessing the relationship between spectral vegetation indices and shrub cover in the Jornada Basin, New Mexico. *International Journal of Remote Sensing*, 14: 3395-3416.

Fisher P. F. and S. Pathirana, 1990. The evaluation of fuzzy membership of land cover classes in the

suburban zone. *Remote Sensing of Environment*, 34: 121-132.

Foody G. M. and D. P. Cox, 1994. Sub-pixel land cover composition estimation using a Linear Mixture Modelling and Fuzzy membership functions. *International Journal of Remote Sensing*, 5(3): 619-631.

Franklin, E., 1994. Discrimination of subalphine forest species and canopy density using digital CASI, SPOT PLA and Landsat-TM data. *Photogrammetric Engineering and Remote Sensing*, 60(10): 233-1241.

Garcia-Haro F. J., M.A. Gilabert, and J. Mela, 1996. Linear spectral mixture modeling to estimate vegetation amount from optical spectral data. *International Journal of Remote Sensing*, 17: 3373-3400.

Green, E. P., P. J. Mumby., A. J. Edwards, and C. D. Clark, 1996. A review of remote sensing for the assessment and management of tropical coastal resources. *Coastal Management*, 21: 1-40.

Hummel, J. W., K. A. Sudduth, and S. E. Hollinger, 2001. Soil moisture and organic matter prediction of surface and subsurface soils using an NIR soil sensor. *Computers and Electronics in Agriculture*, 32: 149-165.

Jensen J. R., 1996. Introductory digital image processing: A remote sensing perspective (2nd edition), Prentice Hall, New Jersey.

Lillesand T. M. and R. W. Kiefer, 1994. Remote Sensing and Image Interpretation. John Wiley and Sons, New York.

Mas, J. F. and I. Ramirez, 1996. Comparison of land use classification obtained by visual interpretation and digital processing. *ITC Journal*, 3-4: 278-283.

Martin, L. R. G., 1989. Accuracy assessment of Landsat based visual change detection methods applied to the rural-urban fringe. *Photogrammetric Engineering and Remote Sensing*, 55: 209-215.

Mather P. M., 1987. Computer processing of remotely sensed images. An introduction. Wiley and Sons, London.

McGwire, K., T. Minor, and L. Fenstermaker, 2000. Hyperspectral mixture modeling for quantifying sparse vegetation cover in arid environments. *Remote Sensing of Environment*, 72: 360-374.

MSSRF, 1995. Pitchavaram mangroves. M.S. Swaminathan Research Foundation, Chennai, India, p.10-11.

Pu, R., B. Xu, and P. Gong, 2003. Oakwood crown closure estimation by unmixing Landsat TM data. *International Journal of Remote Sensing*, 24(22): 4433-4445.

Quarmby N. A., J. R. G., Settle, and K. H. White, 1992. Linear mixture modeling of multitemporal AVHRR data for crop area estimation. *International Journal of Remote Sensing*, 13(3): 415-425.

Ramachandran S., S. Sundaramurthy., R. Krishnamoorthy., J. Devasenapathy, and M. Thanikachalam, 1998. Application of remote sensing and GIS to coastal wetland ecology of Tamil Nadu and Andaman and Nicobar group of islands with special reference to mangroves. *Current Science*, 75(3): 236-244.

Ramsey W., A. Nelson., K. Sapkota., C. Laine, and S. Krasznay, 1999. Using multiple-polarization L-band radar to monitor marsh burn recovery. *IEEE Transactions on Geoscience and Remote Sensing*, 37(1): 635-639.

Rainey, M. P., A. N. Tyler., D. J. Gilvear., R. G. Bryant, and P. McDonald, 2003. Mapping intertidal estuarine sediment grain size distributions through airborne remote sensing. *Remote Sensing of Environment*, 86: 480-490.

Roberts, D. A., M. O. Smith, and J. B. Adams, 1993. Green vegetation, non-photosynthetic vegetation, and soils in AVIRIS data. *Remote*

Sensing of Environment, 44: 255-269.

Roberts D. A., M. Gardner., R. Churn., S. Ustin, and G. Scheer, 1997. Mapping chaparral in the Santa Monica mountains using multiple end-member spectral mixture models. *Remote Sensing of Environment*, 65: 267-279.

Selvam, V., 2003. Environmental classification of mangrove wetlands of India. *Current Science*, 84(6): 757-765.

Settle J. J. and N. A. Drake, 1993. Linear mixing and the estimation of ground cover proportions. *International Journal of Remote Sensing*, 14(6): 1159-1177.

Shanmugam, P., 2002. Multisensor image analysis and sub-pixel classification for improved coastal mapping. Ph.D Thesis, Anna University, Chennai, India.

Smith, M. G., T. Spencer., A. L. Murray, and J. R. French, 1998. Assessing seasonal vegetation change in coastal wetlands with airborne remote sensing: an outline methodology. *Mangroves and Salt Marshes*, 2: 15-28.

Swain P. H. and S. M. Davis, 1978. Remote Sensing: The Quantitative Approach. McGrau-Hill, New York.

Thom, B. G., 1984. Mangrove ecosystem: research methods. UNESCO, Paris, pp.3-17.

Thomson, A. G., R. M. Fuller., T. H. Sparks., M. G. Yates, and J. Eastwood, 1998. Ground and airborne radiometry over intertidal surfaces: Waveband selection for cover classification. *International Journal of Remote Sensing*, 19: 1189-1205.

Ustin, S. L., Q. J. Hart., L. Duan, and G. Scheer, 1996. Vegetation mapping on hardwood rangelands in California. *International Journal of Remote Sensing*, 17: 3015-3036.

Zhu, Z. and D. L. Evans, 1994. U.S. Forest types and predicted percent forest cover from AVHRR data. *Photogrammetric Engineering and Remote Sensing*, 60: 525-531.